# CHARACTERIZATION OF EARTH-ORBITING OBJECTS USING ARTIFICIAL INTELLIGENCE FOR PHOTOMETRIC DATA ANALYSIS

**Gabriele Falco(1), Lucia Mars Sanchez(1), Claudia Reyero Bardelás(1), Marco Acernese(2), Cesar Daniel Enriquez (3)**

*(1) Indra Deimos, Ronda de Poniente, 19, 28760 Tres Cantos, Madrid, Spain, Email: {gafalco, lmars, creyero}@indra.es*
*(2) Indra Deimos, Av. Columbano Bordalo Pinheiro, 75, 1070-061 Lisbon, Portugal, Email: macernese@indracompany.com*
*(3) ETSI Aeronáutica y del Espacio, Universidad Politécnica de Madrid, Pz. Cardenal Cisneros 3, 28040 Madrid, Spain, Email: cesar.enriquez@upm.es*

## ABSTRACT

The growing number of space objects demands improved identification and characterization for effective space traffic management. Accurately characterizing their features is essential for detecting anomalies and understanding behaviour.

Deimos owns and operates a network of ground-based optical sensors that track objects at all altitudes. These high-frequency photometric telescopes provide a cost-effective way to study RSOs by analysing brightness variations from sunlight reflection. The collected data enables the characterization of shape, size, and rotation state under different visibility conditions, crucial for assessing object stability and potential risks.

Machine learning techniques, particularly neural networks, have proven to be a powerful tool to analyse non-linear relationships in data. This study combines classification and regression algorithms to extract patterns and predict RSO characteristics.

To improve training efficiency, both simulated and real data are used. Simulated data forms the algorithm's backbone, while real observations ensure the models generalize effectively to real-world cases, improving prediction reliability.

## 1 BACKGROUND AND RELATED WORK

Classifying and characterizing the properties of space objects is a key objective in Space Situational Awareness (SSA) to enhance knowledge about their state.

To do so, light curve data serves as a powerful tool for uncovering key insights on object behaviour making it an invaluable added resource for real-time monitoring of the space environment. In the frame of photometric data analysis, light curve inversion has been a primarily technique widely used for studying shapes and rotational characteristics of asteroids, which is dating back to the second half of the 20th century [1, 2]. However, when it comes to apply these techniques to artificial satellites, the problem becomes significantly more challenging. RSOs have various shapes, complex attitude controls systems and the reflective properties of each part of the satellite (mainly body and solar panels) vary considerably.

With the latest advancements in optical sensors, detectors and processing technologies, light curve analysis has become a powerful tool for predicting space object features. Many innovative methods have been implemented for extracting satellite features from light curves, but given the strong correlation between shape, size, attitude and materials, predictions are often treated separately by assuming that one (or more) characteristic is known [3,4,5].

In general terms, the brightness of a space object at a given moment depends on its shape, the reflective properties of the surface, its orientation, and how it is illuminated. This illumination is determined by the positions of the Sun, the observer, and the object itself. As a result, the functional relationship between luminosity and the problem's variables is complex and nonlinear.

Moreover, due to the surjective nature of this function, a well-defined inverse function does not necessarily exist. This property is reflected in the fact that different combinations of input variables can result in the same observed brightness. However, the physical evolution of the satellite's state constrains the possible sequences of values that each variable can take. Therefore, a comprehensive analysis of all the measurements comprising the light curve could provide information that would not be obtainable by examining each parameter separately. For this reason, many innovative approaches have explored the possibility to use neural networks as an analysis method, given their ability to extract patterns from large datasets [6, 7, 8].

*Proc. 9th European Conference on Space Debris, Bonn, Germany, 1–4 April 2025, published by the ESA Space Debris Office*
*Editors: S. Lemmens, T. Flohrer & F. Schmitz, (http://conference.sdo.esoc.esa.int, April 2025)*

## 2 FAST PHOTOMETRY OBSERVATIONS

Fast photometry technique allows measuring the flux or intensity of light from space objects at a high frame ratio (several images per second). Usually, the flux of the radiated light is measured by a photodiode or lately through a CCD or CMOS camera attached to a telescope. The incoming light (flux) needs to be calibrated, so converted to instrumental magnitudes. Once the system is calibrated with a known standard object, the further measurements are corrected by atmospheric extinction and extinction coefficients according to the passband of the instrument.

The most important requirements for fast photometric optical cameras are:

- High frame rate
- High sensitivity
- No mechanical shutters
- Fast read-out
- Low noise

The very short exposure times required for detection of very fast LEO objects motion, and the relatively small aperture of the sensors impose some restrictions on the faintest object that can be accurately detected. Moreover, when tracking LEO satellites, in the FoV (Field of View) reference stars background changes very quickly and it is critical to track the object with high accuracy and sensitivity.

Fast photometry final product is the so-called light-curve, that can be interpreted as the fingerprint that the space object leaves at each pass on the detector. When consecutive measurements are taken at frequencies below 1 second (ideally several hertz), they not only enhance light curves through finer sampling but also make it easier to detect rapid, occasional bright variations (glints) and high-speed rotational periods, such as tumbling or high-frequency spinning, as in Figure 2-1.

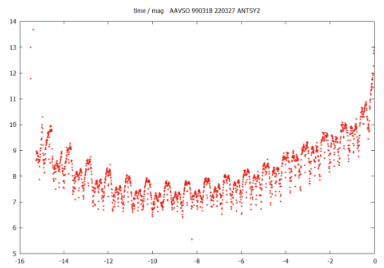

*Figure 2-1: Normalized time vs magnitude of a fast rotator object*

However, sometimes fast photometry is not enough to extract rotational information due to the under-sampling of the rapid brightness variations, as in Figure 2-2. In this case the dispersion of the samples makes the features almost invisible to any approach if seen in time domain. When this happens, it is recommended to switch to the frequency domain (i.e. Fourier analysis or Lomb-Scargle periodograms) or applying epoch folding techniques, which may recover high-frequency details [8].

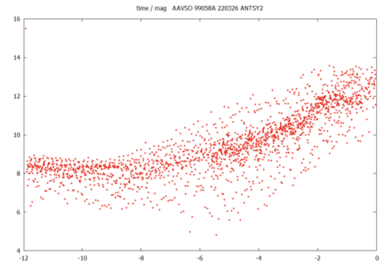

*Figure 2-2: Normalized time vs magnitude of a spinner object (object that rotates faster than the sampling frequency of the sensor)*

Generally, fast photometry is characterized by the following performances:

- > 1Hz – 10Hz (high sampling data rate)
- Accurate pointing / autoguiding
- Applicable to LEO

The geometry of the observation in LEO (as in Figure 2-3) is mainly affected by a fast phase angle variation and large changes in magnitude due to range variations across the track. Indeed, light curves in LEO typically exhibit a parabolic shape, with the brightest point occurring at the satellite's closest approach to the observer, which generally corresponds to the lowest magnitude due to the inverse logarithmic scale.

Given that LEO satellites pass over the telescope site many times at different elevations, azimuth, and illumination conditions, a large variety of light curves can be collected, helping to extract multiple features, especially when applied to constellations. These have indeed the advantage of being made of multiple identical satellites (same shape and surface scattering properties), giving key insights on how the same object behaves under different orientations and illumination conditions.

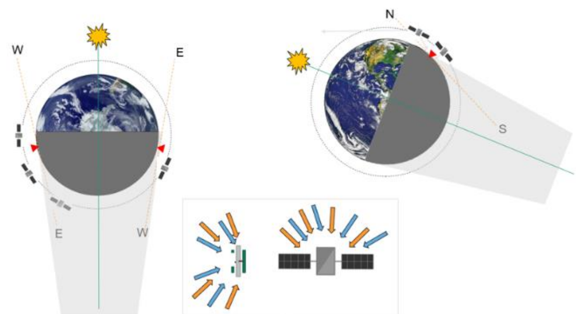


*Figure 2-3: Geometry of LEO satellite observations*

As opposed to LEO, GEO satellites experience slower phase angle variations and maintain a nearly constant observation angle. This means that if a GEO satellite is stabilized, the sensor can only capture a limited area of the object with an angle that is mainly depending on the season. (as in Figure 2-4).

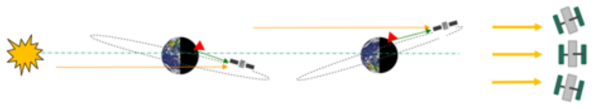

*Figure 2-4: Geometry of GEO satellite observations varying throughout the year*

## 3 DATA COLLECTION AND PROCESSING

This study is intended to exploit the ability of ML algorithms to extract hidden patterns in light curves and provide satellite features. To do so, a large amount of data is required for training given the common rule of "the more data available, the better the predictions the models can make". Due to this strict requirement, the training of ML models has been conducted using two sources: real photometric data collected by the Deimos telescopes and simulated data.

### 3.1 Simulated light curves

Synthetic light curves have been generated using a simulator developed by Deimos. The simulator models satellite orbits using the Simplified General Perturbations 4 (SGP4) method, propagating Two-Line Element (TLE) data to determine the satellite's trajectory. The simulation accounts for visibility constraints, ensuring that the satellite is illuminated by the Sun, is not in Earth's shadow, and the Moon is not in the surroundings of the line-of-sight.

To generate light curves, the simulator employs a tool called POV-Ray, a rendering software that uses the ray tracing technique. It simulates the path of light by tracing rays backward from the observer to the light source, optimizing computational efficiency by only considering rays that reach the observer.

Typically, when a surface is illuminated by the Sun, it reflects the sunlight in both specular and diffuse way. While for specular reflection the incident angle is equal to the reflected angle, for diffuse reflection a Lambert model is used. The most generic way to describe the overall light intensity reflected from surface $i$ and perceived by an observer is:

$$\rho_{total}(i) = \rho_{spec}(i) + \rho_{diff}(i) \qquad (1)$$

The simulator takes in input the satellite's geometry, its material properties and attitude, allowing realistic rendering of how light interacts with the satellite's surface under different illumination conditions. The satellite's body is typically modelled with a balanced mix of diffuse and specular reflection, whereas solar panels are generally treated as entirely specular.

The apparent magnitude of the satellite is extracted from the rendered images by summing pixel intensities, converting them into photon counts, and applying a calibration process to align the results with real observational conditions. The light curve is then obtained by finally determining the magnitude at each time step.

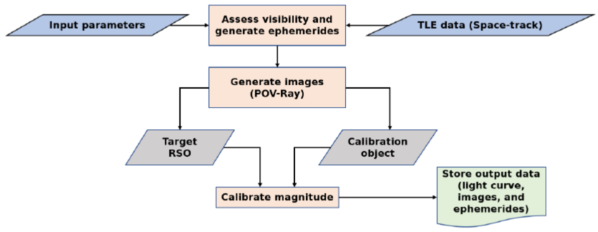


*Figure 3-1: Flowchart of the light curve generation algorithm implemented by the simulator (from [8])*

Due to the large distances between the simulated objects in the scenario, numerical stability issues can arise when generating images with POV-Ray. To address this limitation, a scaling factor is applied to proportionally reducing all distances. Once images are generated, the scaling factor is reversed and the luminosity of the RSO is computed, expressed in terms of apparent magnitude, defined by the following equation:

$$m_v = m_r - 2.5\, log_{10}\left(\frac{B}{B_r}\right) \qquad (2)$$

Where $m_r$ is a pre-defined magnitude of the reference brightness (in this case 21.92), which represents the average sky brightness, B the brightness of the object, that is the total number of photons emitted, and $B_r$ the reference brightness. However, since POV-Ray does not use physical magnitudes, such as the irradiance or the radiant flux, to compute the brightness of the simulated object, a reference calibration object whose actual brightness can be obtained analytically has been used.

Since material prediction is beyond the scope of this activity, each characteristic is simulated based on a fixed material configuration: Multi-layer Insulator, MLI, (which provides satellites with an insulation system that offers high thermal resistance in a vacuum environment) for the satellite body, and GaAs-type reflection (highly polished and predominantly specular) for the solar panels.

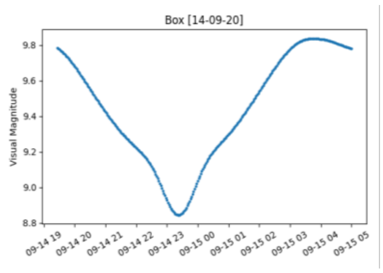


*Figure 3-2: Example of a simulated light curve for a Box-shaped LEO satellite*

### 3.2 Real light curves

Real light curve data has been obtained using Deimos sensors in a fast-photometry mode. These sensors are installed in a remote location with minimal light pollution to ensure high-quality observations. A connected control facility is responsible for monitoring and managing the sensors, ensuring continuous data collection and system functionality.

*Figure 3-3: Deimos Sky Survey sensors*

The sensors collect data each night and multiple objects with different features have been selected which span various characteristics:

- Orbital regime (LEO to GEO)
- Size (extra-small to extra-large)
- Shapes (simple ones like sphere, box, cylinder and box with panels)
- Status (active/inactive if known)

### 3.3 Calibration

Real raw photometric light curves contain valuable information about satellite's brightness variations over time, but they also include systematic errors, observational biases, and noise that can affect the observed satellite magnitude.

To account for variations in exposure time, observed photon counts are calibrated consistently with the real value of exposure time of the sensor.

To account for variations in range, the observed counts are calibrated considering standard values of range (1000km).

In addition, due to the presence of outliers in light-curve data that can sensibly affect subsequent data processing, it is of paramount importance to remove them just after the calibration. Given that magnitudes vs time values may present abrupt changes, peaks and sharp features, the identification of outliers is not straightforward.

The overall calibration process can be summarised with the following steps:

- Calibration by exposure time (sensor-dependent)
- Subtraction of calibrated background counts
- Calibration by range (standard 1000km)
- Calibration by atmospheric extinction
- Outlier's removal

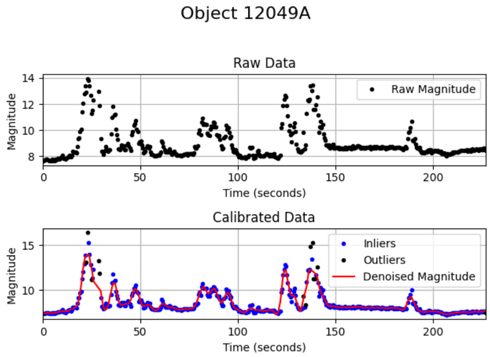


*Figure 3-4: Light curve calibration (top: raw data, bottom: calibrated data)*

The complexity of this task lies in the fact that the brightness variation of a real object can exhibit spikes and abrupt changes. For example, reflections from the solar panels of some satellites can cause flares, resulting in sudden variations in brightness. This makes it difficult to distinguish between true anomalies and behaviours that may occur in a real object. In the current implementation, the removal of anomalous values is carried out in four steps:

1. Values that deviate more than 3 standard deviations from the mean of the values recorded during the satellite's entire observation window are removed
2. The Butterworth filter is applied to eliminate the noise
3. Values that deviate more than 3 standard deviations from the mean of the smoothed data are removed again
4. The Butterworth filter is applied once more to suppress the noise, and the remaining anomalous values are removed.

The Butterworth filter [9] is a mathematical technique that allows low-frequency components of a signal to pass through, while reducing the amplitude of components whose frequency is greater than a specified cutoff value. When applied to the light curve, it produces a smoothing effect that removes random variations caused by measurement errors or noise, thereby facilitating the detection of anomalous values. Figure 3-4 shows an example of the calibration process, displaying the removed anomalous values and the result. It also includes a comparison with an uncalibrated light curve.

## 4 MACHINE LEARNING APPROACH

ML tools extend the capability of exploiting light curve analysis for precious information regarding space object's characteristics. Deep learning techniques have demonstrated to be reliable in many space practices when the models are correctly and logically implemented with the proper data set and configuration parameters.

Recurrent Neural Networks (RNNs), particularly Long Short-Term Memory (LSTM) architectures, have proven to be highly effective in handling time-sequenced data, such as light curves, as they enable the retention of important information over time. These networks use memory cells to maintain important information from earlier sequences, while using gates to control the flow of information, deciding what enters or leaves the memory cells giving a better understanding of long-term dependencies. The network used can be summarised into three main layers:

- **Input data**: the original data the network will extract the information from (i.e. light curves)
- **Hidden layers**: the layers that extract the characteristics of the data to learn patterns and make predictions (LSTM model)
- **Output data**: the prediction made by the network based on the learned characteristics of the input data (i.e. Shape, Size, and Status)

For each characteristic analysed, the Machine Learning framework is built using Keras, which is a model-level library built up on TensorFlow providing high-level building blocks for developing deep learning models.

In ML activities it is common to use a batch of training samples composed by inputs $x$ and targets $y$, where the network is run on $x$ to obtain a prediction of $y$. After that, the model computes the loss on the batch, calculates the gradient of the loss and updates the parameters (weights and biases) in the opposite direction of the gradient to minimize the loss.

In the context of this research, two main types of networks have been considered:

- Binary classification: The output layer uses a sigmoid activation function to produce a probability between 0 and 1 representing the likelihood of the input belonging to the positive class. Then a threshold is used to make the final classification decision.
- Multiple class classification: Sorts the input data into several categories and trains the network. When an input is processed, the network uses a SoftMax activation function to predict the probability distribution of the data through all the categories and the category with the highest probability will be the result of the prediction
- Regression: predicts a continuous numerical value that represents a real-world value dependent on the input data given

The high-level scheme of the process providing the prediction of the three satellite characteristics analysed is shown in Figure 4-1. The calibrated light curve is represented as a time series of four variables: epoch, magnitude, range, and phase angle.

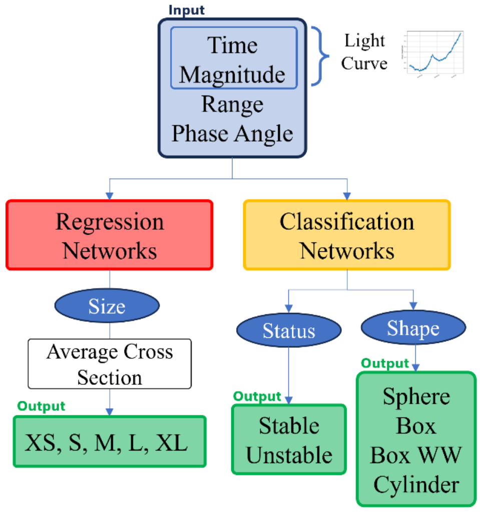


*Figure 4-1: Prediction flow of the three characteristics: size, shape, and status*

Shape and Status feature estimations are based on a classification network which classifies both into multiple categories:

- Shape**:** four common and simple shapes are studied, such as sphere, cylinder, box, and box with panels. These configurations have been chosen as they are commonly used geometries in satellite design.
- Status**:** two simple cases are considered, stable and unstable satellite

On the other hand, size is predicted through a regression approach that depends on the average cross-section, from which four different classes are evaluated (XS, S, M, L, XL)

Finally, the computation of the average cross-section has been performed using the ESA CROC tool, which is part of the DRAMA software. [10]

### 4.1 Shape

The classification of satellite geometries in this study is approached as a categorization problem, where each object is assigned to one of the predefined shape categories. To generate the preliminary dataset using the light curve simulator, four fundamental satellite geometries have been selected: sphere, box, box with solar panels, and cylinder. These configurations were chosen due to their widespread use in satellite design.

Figure 4-2 and Figure 4-3 illustrate these geometries and provide examples of the corresponding light curve patterns. The curves shown in these figures correspond to a specific observation period, and their shape and magnitude may vary under different viewing conditions.

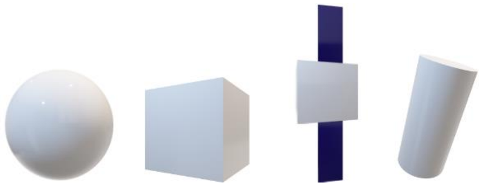

*Figure 4-2 - Satellite Geometries*

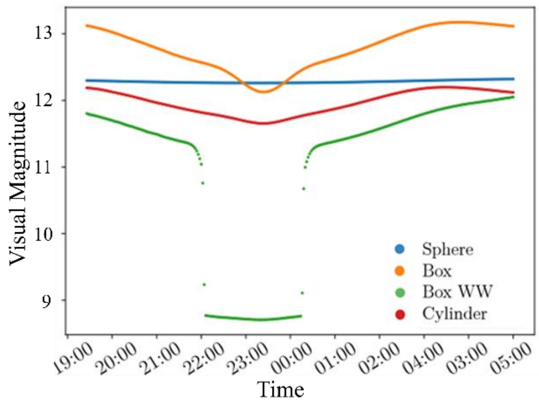


*Figure 4-3: Simulated light curves of the different geometries (a magnification factor has been applied to the objects in the image for illustrative purposes to get larger and slower variations of magnitude).*

The expected magnitude variations are observed in the light curves for each geometry. For spherical objects, the magnitude remains nearly constant throughout the observation window, as their symmetrical shape ensures that their reflective properties do not change with viewing angle.

For both the box and the cylinder, a decrease in magnitude is observed around the midpoint of the observation period. This is due to an increase in the amount of direct sunlight reflected during that phase, as illustrated in Figure 4-4. The figure presents three scaled images for each geometry, corresponding to different moments of the observation period.

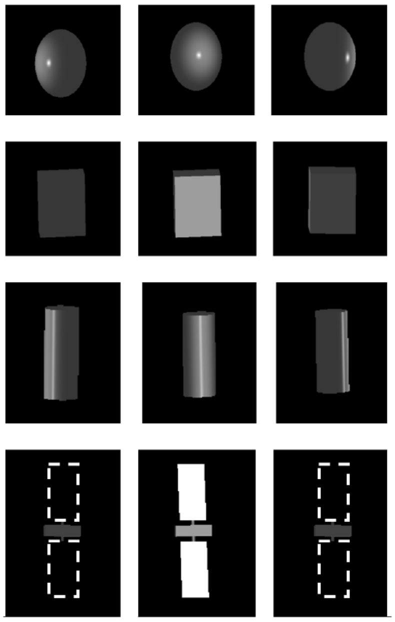

*Figure 4-4: Illumination of the four geometries for one night (19:30, 23:30 and 5:00). From top to bottom: sphere, box, cylinder and box with wings.*

The box with wings exhibits a more pronounced drop in magnitude, which is attributed to the direct reflection of sunlight on the solar panels. This effect significantly increases the illuminated surface area, leading to a noticeable reduction in the measured magnitude. It must be noticed that for representative purposes scenarios have been magnified and for this reason the glint in Figure 4-3 generated by the box with wings lasts two hours, which does not reflect a real behaviour.

To develop this multiple-class classification model, a categorical cross-entropy loss function has been used.

$$L = -\sum_{i=1}^{C} y_i log\hat{y}_i \tag{3}$$

In this function C is the number of classes, $y_i$ is the true probability for class $i$ (typically 0 or 1) and $\hat{y}_i$ is the predicted probability. It measures the dissimilarity between both values and penalizes the model heavily when it gives a low probability to the correct class. This helps the model to output high confidence in the true class.

## 4.2 Size

An object composed of the same materials but with a larger size will reflect more light, and as expected, its brightness will be higher. As shown in Eq. 2, the greater the object's magnitude, the lower its brightness, meaning that larger objects will have lower magnitude values.

The size of each object in this work is determined based on its average cross-section, which is used as input for a regression model. To facilitate interpretation, the predicted values are mapped into five discrete size categories: XS, S, M, L, and XL. These thresholds vary depending on the object's geometry, as shown in the following table:

*Table 1: Size category thresholds (in $m^2$) based on average cross-section for different object geometries.*

| | XS | S | M | L | XL |
|---|---|---|---|---|---|
| **Sphere** | < 0.1 | [0.1 - 0.5] | (0.5 - 1] | (1- 2] | > 2 |
| **Box** | < 0.1 | [0.1 - 0.5] | (0.5 - 1] | (1- 2] | > 2 |
| **Box WW** | < 0.1 | [0.1 - 1] | (1 - 3] | (3 – 5] | > 5 |
| **Cylinder** | < 0.1 | [0.1 - 1] | (1 - 3] | (3 – 5] | > 5 |

For this regression model, the mean squared error has been used as loss function.

$$MSE = \frac{1}{n}\sum_{i=1}^{n}(Y_i - \hat{Y}_i)^2 \tag{4}$$

In this function, $n$ is the number of observations, $Y$ is the model's prediction, and $\hat{Y}$ is the true value. It squares the difference between both values, which gives more weight to outliers. This is very useful for gradient-based optimization because it gives more weight to substantial prediction deviations.

### 4.3 Rotation State

In general, inactive satellites rotate uncontrollably due to a failure in their control system, a faulty design, or environmental factors. Accurately predicting the rigid body dynamics is a complex task given that it can be perturbed by both internal and external torques. External torques come from the interaction of the satellite with the space environment (gravity gradient, magnetic, solar radiation…) and their combined effects can be difficult to be modelled and strongly affect the prediction.

Moreover, as discussed in section 2, telescopes have a limited capacity to obtain high-cadence images of satellites to detect very fast rotators. Objects that rotate very quickly (as in Figure 2-2) present indeed two main challenges:

- generating a data set dense enough in time
- detecting the rotation pattern within it

The first one is related to both computational limits of the simulator supporting the ML models, and the physical limits of the real sensor. The second depends on the reflections of the light on the object, which could appear blurry and be confused with background noise if ML algorithms are not properly trained and images calibrated against noise.

The simulated data generated use a simpler body dynamics approach, assuming an initial stabilized satellite in Local Vertical-Local Horizontal reference frame and propagate its rotation in time by applying an angular velocity vector $\vec{\omega}$, without considering any external torque and with a rate within the detectable limits of Deimos' sensors.

This model focuses then on identifying satellite stability based on the angular velocity rate predicted through a binary classification (stable/unstable). If the calculated angular rate results to be lower than 1deg/s, then the satellite is considered stable. This margin has been accounted for due to the inherent bias and uncertainty in the statistical predictions generated by the ML models.

To help the model obtain the best predictions possible, Bidirectional LSTM layers have been used. These layers process the sequence in a forward and backward manner. Using this technique can help identify the patterns in brightness fluctuation better because sometimes, rotation characteristics might become more apparent after viewing the light curve holistically rather than sequentially.

In a binary classification model where the data has characteristics like the ones presented here, the threshold used for the predictions holds a very important role in obtaining good results. To optimize its value, it has been obtained by maximizing the F-1 score metric, meaning that the threshold corresponding to the highest F-1 score values is the one selected. This ensures that the model considers any possible class imbalance.

For this binary classification model, a binary cross-entropy loss function has been used.

$$BCE = -\frac{1}{N}\sum_{i=1}^{N} y_i \log\big(p(y_i)\big) + \\ + (1 - y_i)\log\big(1 - p(y_i)\big) \tag{5}$$

In this function, $y_i$ is the true binary label (either 0 or 1), and $p$ is the predicted probability of the positive class. This formula measures the dissimilarity between the true labels and the predicted probabilities, so it heavily penalizes confident and wrong predictions. This makes it very effective for binary classification tasks, creating a continuous error surface for model training.

## 5 RESULTS AND DISCUSSION

The following section presents the performance evaluation of the proposed machine learning models for shape classification, size estimation, and stability prediction of RSOs.

All the networks have been trained using a total amount of light curves that vary between 1000 and 2000 mostly composed of simulated ones, with a small number of real ones. Then, from all the data gathered, 10% was used as the test dataset, and from the remaining 90%, another 25% was used for validation.

To assess the capability of the models, the results are analysed in terms of:

- *Accuracy:* represents the correct values out of all the predictions made. It is used to analyse classification models, as it provides a general measure of overall performance. A value closer to 1 indicates a higher number of correct predictions. However, in cases where the dataset is imbalanced, accuracy may not properly reflect the true performance of the model, as it can be biased toward the majority class. For this reason, accuracy is not used as the sole evaluation metric in our classification models.
- *Area Under the Curve (AUC):* used in classification models, it represents the area under the Receiver Operating Characteristic curve (ROC) which shows how the model balances correctly identifying positive cases (true positives) while avoiding false alarms (false positives) at different probability thresholds. This allows the AUC value to be indifferent to class imbalance regardless of the chosen threshold. If its value is close to 1, the model would have near-perfect classification but if its value is below 0.5 it would indicate that the model is making random guesses.
- *Mean absolute error (MAE):* commonly used to evaluate regression models by measuring the average absolute difference between the predicted and the real values. It indicates how far the predictions are from the true values, without considering if the errors are positive or negative. A lower MAE indicates more accurate predictions, while a higher MAE suggests bigger deviations from the actual values. This metric is not sensitive to outliers; therefore, it is best to be complemented with other metrics.
- *Mean squared error (MSE):* commonly used in regression models, it measures the average of square differences between the predicted and the real values. Due to the squaring operation, MSE is more sensitive to outliers and large deviations compared to MAE. Its value is always positive, with lower values indicating a better model performance. Although MSE cannot be directly interpreted in the units of the output data, it serves as an effective loss function due to its desirable mathematical properties, such as differentiability, which facilitates optimization in machine learning models [11].

Differences between training and validation performance are discussed, highlighting limitations and potential areas of improvement. Additionally, the impact of orbital regime and object stability on model performance is examined, addressing the challenges associated with characterization of space objects.

### 5.1 Shape

Table 2 presents the classification performance of the model in determining the shape of RSOs under different orbital regimens and stability conditions. The high accuracy in training shows effective learning, while the drop in validation accuracy, particularly in stable LEO cases, may indicate a lower generalization in shape differentiation when rotational variability is lower. Indeed, when the object is stable may happen that not all shape features are visible during a few passes. Let's take as an example the box with panels: if no glint from solar panels is appearing in the light curve, the ML model can easily misclassify it as a simple box-shaped object.

*Table 2: Shape characterization*

| Regime | Status | Training Stage | Accuracy | AUC |
|---|---|---|---|---|
| LEO | Stable | Training | 0.983 | 0.999 |
| | | Validation | 0.696 | 0.838 |
| | Unstable | Training | 0.979 | 0.997 |
| | | Validation | 0.865 | 0.937 |
| GEO | Stable | Training | 0.864 | 0.981 |
| | | Validation | 0.828 | 0.975 |
| | Unstable | Training | 0.965 | 0.997 |
| | | Validation | 0.940 | 0.971 |

### 5.2 Size

The model, whose results are shown in Table 3, demonstrates low MAE and MSE values for size predictions of spherical objects, suggesting robust generalization across different orbital regimes. The consistently low validation errors indicate that the model effectively captures the relationship between observed brightness variations and object cross-sectional area for this geometry.

In GEO, the results appear to be of lower quality due to the scarcity of real spherical examples in orbit, making it difficult to generalize predictions. Furthermore, for smaller objects, slight size differences are hard to distinguish, as the satellite occupies only a few pixels in the image, limiting detectable variations in brightness.

*Table 3: Size predictions of Sphere*

| Regime | Status | Training Stage | MAE | MSE |
|---|---|---|---|---|
| LEO | Stable | Training | 0.0148 | 0.002 |
| | | Validation | 0.0127 | 0.002 |
| GEO | Stable | Training | 0.979 | 1.317 |
| | | Validation | 0.997 | 1.368 |

Box-shaped satellites size prediction in LEO gets accurate results both in stable and unstable configuration, as shown in Table 4. The slight difference between the training and validation indicates that the model fits both training and validation dataset.

On the other side, it exhibits significantly higher errors in GEO scenarios compared to LEO, particularly in the stable case. This discrepancy suggests that the model may struggle with variations in phase angle and illumination conditions in GEO, where geometry remains nearly constant with respect to the observer.

Additionally, unstable cases in both LEO and GEO show lower values in both metrics. This may be because unstable objects, as they rotate, expose different faces of the satellite over time. This change in the observed surface provides more diverse information about its structure, making it easier for the model to identify key features. On the other hand, stable objects maintain a fixed orientation, limiting the amount of visible information and potentially making any estimation about the satellite's characteristics more challenging.

This demonstrates that stability or low variability is not always beneficial. In many cases, either due to the orbital regime in which the satellites are located or the instability they exhibit, they provide more information to the observer, allowing the models to learn more effectively. Conversely, highly repetitive data without distinctive features contributes less to the model's training and learning process.

*Table 4: Size predictions of Box*

| Regime | Status | Training Stage | MAE | MSE |
|---|---|---|---|---|
| LEO | Stable | Training | 0.0003 | 1.708 |
| | | Validation | 0.0005 | 2.745 |
| | Unstable | Training | 0.0006 | $7.65 \cdot 10^{-7}$ |
| | | Validation | 0.002 | $4.42 \cdot 10^{-6}$ |
| GEO | Stable | Training | 0.402 | 0.229 |
| | | Validation | 0.406 | 0.239 |
| | Unstable | Training | 0.221 | 0.0903 |
| | | Validation | 0.162 | 0.052 |

The results for box-wing objects (in Table 5) show increased prediction errors in stable GEO cases, which may be attributed to their high dependency on phase angle variations. The lower error values in unstable conditions suggest that rotational motion introduces more distinguishable light curve patterns, in particular when the shape is more complex. Indeed, the same insights can be extracted both for box and box with panels case.

*Table 5: Size predictions of Box with Wings*

| Regime | Status | Training Stage | MAE | MSE |
|---|---|---|---|---|
| LEO | Stable | Training | 0.095 | 0.101 |
| | | Validation | 0.133 | 0.211 |
| | Unstable | Training | 0.0134 | 0.0013 |
| | | Validation | 0.008 | 0.0001 |
| GEO | Stable | Training | 0.571 | 0.701 |
| | | Validation | 0.579 | 0.699 |
| | Unstable | Training | 0.197 | 0.066 |
| | | Validation | 0.163 | 0.035 |

For cylindrical objects the model exhibits high accuracy in size estimation in LEO regime, with low prediction errors in the stable case, as in Table 6. However, the increased errors in unstable and GEO cases suggest that cylindrical geometries introduce complex reflection dynamics that are not fully captured by the current model. Additionally, not so many cylindrical objects are currently deployed in the GEO region (mostly are GTOs, like rocket bodies), which limits the collection of real data cases.

*Table 6: Size prediction of cylinder*

| Regime | Status | Training Stage | MAE | MSE |
|---|---|---|---|---|
| LEO | Stable | Training | 0.0002 | $8.783\cdot10^{-8}$ |
| | | Validation | 0.0004 | $1.961\cdot10^{-7}$ |
| | Unstable | Training | 0.124 | 0.104 |
| | | Validation | 0.141 | 0.107 |
| GEO | Stable | Training | 0.5955 | 0.7454 |
| | | Validation | 0.708 | 1.814 |
| | Unstable | Training | 0.168 | 0.055 |
| | | Validation | 0.0679 | 0.008 |

### 5.3 Stability

The stability classification model demonstrates higher accuracy in the GEO regime compared to LEO. The reduced validation accuracy in LEO suggests that rapid changes in illumination and viewing geometry introduce ambiguities in the light curve patterns, potentially complicating stability assessment. Incorporating additional temporal features or higher-frequency photometric sampling could mitigate these limitations in LEO.

*Table 7: Stability Predictions*

| Regime | Training Stage | Accuracy | AUC |
|---|---|---|---|
| LEO | Training | 0.704 | 0.695 |
| | Validation | 0.673 | 0.574 |
| GEO | Training | 0.816 | 0.833 |
| | Validation | 0.838 | 0.845 |

It is important to note that a satellite's state cannot be fully assessed based on a single-track prediction. Instead, the characterization process takes a more comprehensive approach, considering the satellite's past, present, and future evolution. Multiple consecutive predictions can either increase confidence in the estimation or prompt a reassessment if the state changes.

### 5.4 Test cases

To assess the performance of the trained neural networks, real light curves were used as a test cases, and the resulting predictions were analysed.

The first object to be analysed is a LEO satellite, whose track is shown in Figure 5-1. It has been identified as a Box with Wings with an extra-large (XL) size and classified as stable. This classification aligns with the object's known properties, as it is indeed a Box with Wings and confirmed to be stable. Moreover, its actual average cross-section is 10.3 m², which, according to the size categories defined in Table 1, falls within the XL range, further validating the accuracy of the model's prediction.

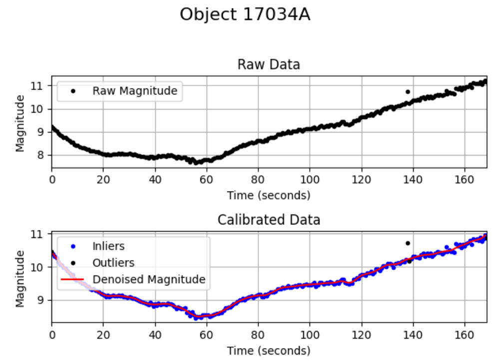


*Figure 5-1: Example of a LEO Real Light Curve for Model Evaluation (top: raw data; bottom: calibrated data)*

The second object, shown in Figure 5-2, is a GEO satellite observed at different intervals throughout the night. It has been classified by the models as a Box with Wings of extra-large size and stable. This classification is consistent with the satellite's known characteristics. Its actual average cross-section, estimated at 28.6 m², also falls within the XL size category, confirming that the model successfully characterizes this satellite as well.

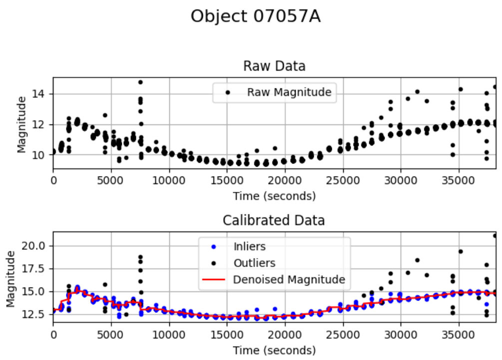


*Figure 5-2: Example of a GEO Real Light Curve for Model Evaluation (top: raw data; bottom: calibrated data)*

Beyond individual classification cases, it is also crucial that satellites are consistently characterized correctly across different observations, rather than just in a single instance. To assess this, the same object was analysed on multiple nights: 20th of February, 4th of May, and again on the 14th of May. The model consistently classified it as a Box with Wings, extra-large in size, and stable across all nights. This consistency over multiple observations reinforces the reliability of the classification and highlights the importance of maintaining accurate characterizations under varying observation conditions, visibility scenarios, and different times of the year. Ensuring stability in predictions is key for long-term satellite monitoring, and achieving this robustness requires a dataset that covers as many real-world cases as possible.

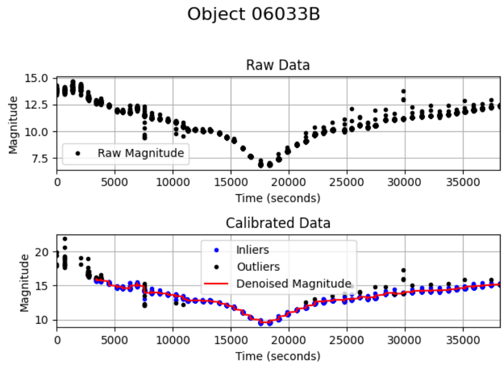


*Figure 5-3: Light curve of a GEO object, analysed across different nights*

Finally, a fourth object was tested where the model's classification appears to be less accurate. The object is part of the cylindrical Meteosat family and in Figure 5-4 a complex light curve has been observed throughout an entire night, with inconsistent and sparse data. This GEO satellite was correctly identified as a stable cylinder in previous observations, but in this case was misclassified as an unstable Box with Wings. This demonstrates that the model can make accurate predictions but, in some cases, lacks full consistency.

To enhance accuracy, the model needs:

- additional real data
- more accurate synthetic satellite model simulation (which sometimes has appendices or complex reflective parts playing an important role on the total brightness)

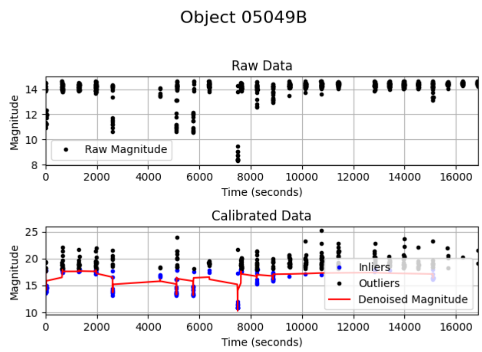


*Figure 5-4: Stable cylindrical GEO satellite incorrectly identified as an unstable Box with Wings.*

## 6 CONCLUSIONS

This work reinforces the effectiveness of AI in enhancing the characterization of Earth-orbiting objects through photometric data analysis. The results highlight AI ability to uncover previously unrecognized patterns with remarkable accuracy, confirming its role as a powerful tool in space situational awareness. This work helps and contribute to a more efficient monitoring and management of the space domain, ensuring the safety of orbital operations.

As a proposal for future enhancements of this analysis, refining ML models with more data, investigate new approaches, and simulate more accurately satellite characteristics can make predictions more consistent. To give a more comprehensive analysis of the satellite status, together with the mentioned characteristics, also attitude estimation models can be implemented, building the backbone for a complete database of satellite status that can be constantly monitored over time. The complexity in attitude information collection is that for RSOs this is usually not disclosed. For active satellites, owners rarely publish it, while for most defunct spacecraft and debris, it remains entirely unknown. Exploring the possibility of AI to understand attitude status from light curve patterns is one of the biggest challenges in characterization.

Finally, integrating even more AI in photometric data analyses and operations could enable the early detection of anomalies or unusual trends in collected data. Automating this monitoring process would in future allow for timely intervention (automatic warning messages can be generated) and reduced manual workload for operators.

## 7 REFERENCES

1. Ostro, S. J., & Connelly, R. (1984). Convex profiles from asteroid lightcurves. *Icarus*, *57*(3), 443-463.

2. Barucci, M. A., & Fulchignoni, M. (1983). On the inversion of asteroidal lightcurve functions. In *Asteroids, Comets, and Meteors* (pp. 101-105).

3. Vananti, A., Guthruf, D, Lu, Y., Schildknecht, T., (2021). Estimation of reflective properties from light curves of a H2A rocket body. Proceedings of 8th European Conference on Space Debris, ESA/ESOC, Darmstadt, Germany, 2021

4. Earl, M.A., Wade, G.A., Observations and analysis of the apparent spin period variations of inactive boxwing geosynchronous resident space objects, Proceedings of 65th International Astronautical Congress, Toronto, Canada, 2014

5. Wetterer J, Jah M. Attitude estimation from light curves. J Guid Control Dyn. 2009;32(5):1648-1651

6. Kerr E, Falco G, Maric N, Petit D, Talon P, Petersen C et al. Light curves for GEO object characterization.

Proceedings of the 8th European Conference on Space Debris, ESA/ESOC, April 2021, Darmstadt (Germany)

7. Enríquez C D, Amato D. Application of LSTMs to the light curve inversion problem. Preprint AAS 23-337. 33rd AAS/AIAA Space Flight Mechanics Meeting: 14th-19th January 2023; Austin (USA). American Astronautical Society

8. Gallego, Á. (2023). RSO Characterization and Attitude Estimation with Data Fusion and Advanced Data Simulation Ángel Gallego, Carlos Paulete, Marc Torras, Adrián de Andrés and Alfredo M. Antón.

9. Butterworth, S. On the Theory of Filter Amplifiers. Experimental Wireless and the Wireless Engineer. 1930;7(85):536-541.

10. Home · Space Debris User Portal. (n.d.). SDUP. https://sdup.esoc.esa.int/

11. Chollet F. Deep learning with Python. Shelter Island: Manning Publications Co; 2018